ORIGINAL RESEARCH

Single-walled carbon nanotubes loaded hydroxyapatite–alginate beads with enhanced mechanical properties and sustained drug release ability

L. B. Sukhodub[1] · L. F. Sukhodub[1] · M. O. Kumeda[1] · Yu. I. Prylutskyy[2] · M. V. Pogorielov[1] · M. P. Evstigneev[3] · V. V. Kostjukov[3] · N. Y. Strutynska[2] · L. L. Vovchenko[2] · S. V. Khrapatiy[2] · U. Ritter[4]

Abstract

Single-walled carbon nanotubes (SWCNTs) containing biomaterial with enhanced mechanical properties for the potential orthopedic application were synthesized and investigated. X-ray diffraction and X-ray fluorescence analysis were indications of the formation of calcium-deficient (Ca/P = 1.65) hydroxyapatite (HA) with a small carbonate content under influence of microwave irradiation. The investigated mechanical properties (maximal relative deformation, compressive strength and Young's modulus) of SWCNT loaded HA–alginate composites confirm their dependence on SWCNTs content. The compressive strength of HA–alginate–SWCNT and the HA–alginate control (202 and 159 MPa, respectively) lies within the values characteristic for the cortical bone. The addition of 0.5% SWCNT, in relation to the content of HA, increases the Young's modulus of the HA–alginate–SWCNT (645 MPa) compared to the SWCNT-free HA–alginate sample (563 MPa), and enhances the material shape stability in simulated physiological conditions. Structural modeling of HA–alginate–SWCNT system showed, that physical adsorption of SWCNT into HA–alginate occurs by forming triple complexes stabilized by solvophobic/van der Waals interactions and H-bonds. The high-performance liquid chromatography demonstrated the influence of SWCNTs on the sustained anaesthesinum drug (used as a model drug) release (456 h against 408 h for SWCNT-free sample). Cell culture assay confirmed biocompatibility and stimulation of osteoblast proliferation of 0.05% and 0.5% SWCNT-containing composites during a 3-day cultivation. All these facts may suggest the potential possibility of using the SWCNT-containing materials, based on HA and alginate, for bone tissue engineering.

Keywords Single-walled carbon nanotubes · Hydroxyapatite · Alginate · Mechanical properties · Drug release

Introduction

Bone tissue defects and fractures due to vehicular accidents, cancer, bone tissue necrosis or rheumatic disease have now become a global and very important issue. The system, where hydroxyapatite (HA) nanocrystals orderly embedded in the collagen matrix with self-assembly of their components, endows natural bone with a hierarchical architecture and excellent mechanical properties (Tang et al. 2013). Calcium phosphate ($CaPO_3$) materials, including HA, are widely used for bone regeneration owing to their biocompatibility and osteoconductivity. 3D $CaPO_3$ porous forms have proven to be useful in bone tissue engineering by providing favorable construction for cell growth and differentiation (Sharma et al. 2014). However, the typical brittleness and low fracture toughness of HA have restricted its applications for high load-bearing implants (Khalid et al. 2013; Van Dijk et al. 1981). Since a bone is subjected to mechanical load, it is crucial that a material used for regeneration of hard tissues has appropriate strength properties to support the applied loads. Therefore, a hybrid material containing organic and inorganic constituents may be better suited for large variations of composites. Natural and synthetic polymers serve as a physical matrix for HA immobilization and are extensively used for constructing biomaterials due to their high

✉ M. P. Evstigneev
max_evstigneev@mail.ru

[1] Sumy State University, Sumy, Ukraine

[2] Taras Shevchenko National University of Kyiv, Kiev, Ukraine

[3] Sevastopol State University, Sevastopol, Crimea

[4] Technical University of Ilmenau, Ilmenau, Germany

biocompatibility and low toxicity (Sukhodub et al. 2018). Bone regenerative medicine often uses proteins such as collagen, fibrin and polysaccharides such as alginate, chitosan, hyaluronic acid. Alginate is a binary copolymer containing (1–4)-linked β-D-mannuronate and α-L-guluronate residues in varying proportion and order. Alginates are abundant in nature and are known as structural components of marine brown algae and as capsular polysaccharides in some soil bacteria (Sakai and Kawakami 2007). They can undergo gelation with divalent cations under very mild conditions, suitable for biomacromolecules and living cells (Beyer et al. 2010; Boontheekul et al. 2005; Lee and Mooney 2012; Li et al. 2005).

To improve the mechanical properties of biopolymer–HA composite, its structure may be reinforced with materials such as carbon nanotubes (CNTs), that belong to the group of the toughest materials ever discovered (Gopi et al. 2013; Iijima 1991; Li et al. 2007; Reich et al. 2008; Ritter et al. 2012) and exhibit resistance to aggressive acid and alkaline media without changing their structure (Li et al. 2015). CNTs consist of one or several graphitic shells, wrapped into a cylindrical tube, and are divided into two groups: multiwalled (MWCNTs) and single-walled (SWCNTs) CNTs (Reich et al. 2008). Recently (Sukhodub et al. 2018), we investigated the mechanical properties of the HA–alginate composite containing 0.04% MWCNT + Fe and showed that the material is characterized by a high compressive strength (168 MPa) compared to a cortical bone.

Despite the fact that CNTs are used in biomedicine for cell visualization, drug delivery and bone tissue engineering, there are contradictory views on their toxicity (Kurantowicz et al. 2017; Minchenko et al. 2018; Prylutska et al. 2008; Singla et al. 2019). It has been shown that in blood stream, some types of CNTs do not cause negative effects, consequently they are potentially suitable for delivery of drugs or biologically active compounds (Buchelnikov et al. 2014; Liu et al. 2009; Raphey et al. 2019). Low doses of CNTs doped HA nanocrystalline powders do not significantly decrease G-292 cell viability and do not induce oxidative stress after 2 days of exposure (Constanda et al. 2016). High cytotoxicity of CNTs, associated with low homogeneity in the solution, restricts their use in medicine (Andón and Fadeel 2013; Cataldo and Da Ros 2008; Li et al. 2017; Radchenko et al. 2013; Tran et al. 2009). CNTs can be exploited to improve drug delivery due to their ability to interact with biomolecules and to cross cell membranes (Kam et al. 2005; Matyshevska et al. 2001; Prylutska et al. 2012, 2013; Wilczewska et al. 2012). Several factors make it possible to use CNTs as a vehicle to transport drugs into cells, viz. surface properties, hydrophilicity, size and shapes (Cataldo and Da Ros 2008; Harik 2017).

The purpose of this work was to obtain biocomposite material with increased mechanical properties, based on HA,

alginate and SWCNTs in the form of 3D beads for potential application in bone tissue engineering. To avoid bacterial contamination of the surgical bone areas, the material should contain drugs. Therefore, one of the tasks was to study properties of the composite as a drug carrier along with its drug release ability. Taking into account the possible toxicity of CNTs, the effect of the synthesized material on the survival of cells in the nutrient medium was also studied.

Materials and methods

Materials

Calcium nitrate tetrahydrate $Ca(NO_3)_2 \cdot 4H_2O$, diammonium dihydrophosphate $((NH_4)_2HPO_4)$, ammonium hydroxide NH_4OH, calcium chloride $CaCl_2$ and pharmaceutical Anaesthesinum (AnS) were purchased from Sinopharm Chemical Reagent Co., Ltd; Sodium Alginate (low viscosity, E407) was purchased from Sanpu Chemical CO., Ltd, Shanghai, China. All reagents were of analytical grade and used as purchased.

Preparation and characterization of HA–alginate–SWCNT composite

Fabrication of SWCNTs

The fabrication of SWCNTs was carried out using graphite electrodes in He atmosphere (700 mbar) by means of arc-discharge technique. For the synthesis process, a hollow in anode was drilled and filled afterwards with powder of catalyst (graphite, 1% Y_2O_3, 4.2% NiO). The arc-discharge was performed with the current of 150 A. The fabricated SWCNTs were treated with hot concentrated hydrochloric acid (6 M) in reflux condenser to remove contaminants, such as amorphous carbon and metallic catalyst particles. The analysis of fabricated SWCNTs was carried out by means of AAS and TG techniques for the estimation of metal nanoparticle impurities and overall content of impurities, respectively (Korolovych et al. 2014; Ritter et al. 2007). In the fabricated SWCNTs, only traces of nickel were detected by means of AAS, while TG experiments demonstrated that the residue of less than 0.3% remained unburned at about 1050 °C.

Preparation of HA hydrogel

HA hydrogel was obtained using a wet chemical co-precipitation method under microwave (MW) influence (Stanislavov et al. 2018). Briefly, for HA synthesis 50 mL of $Ca(NO_3)_2 \cdot 4H_2O$ (0.167 M) and 50 ml of $(NH_4)_2HPO_4$ (0.1 M) were used. Ammonium hydrophosphate was added

dropwise to the calcium nitrate tetrahydrate. The pH value of the mixture was adjusted to 10.5 by addition of ammonia solution under stirring. 100 mL of the obtained suspension was transferred to the MW oven consumer (Samsung M1712NR) for its MW irradiation within 3 min. Then, the product was cooled at room temperature in the closed, but not sealed volume. After being washed, the solid fraction of the sample was separated by centrifugation. The moisture content of the resulting HA hydrogel was about 90%.

Preparation of HA-alginate and HA–alginate–SWCNT beads. 0.75 g of sodium alginate was dissolved in 50 mL of deionized water at 37 °C for 5 h to form 1.5% (w/v) solution. 0.0025 g of SWCNTs in the form of a fine powder was added to the alginate solution to obtain the concentration of SWCNTs in alginate solution of 0.05 mg/mL. The mixture was sonicated at low (90 W) power for 20 min. As a result, a homogeneous and stable alginate–SWCNT colloidal suspension was formed. After that, HA hydrogel (in Sect. "Preparation of HA hydrogel") was gradually added to alginate–SWCNT suspensions at 1:1 weight ratio and sonicated for 5 min. Mixtures were dripped into 0.25 M calcium chloride solution for a period of 24 h. The formed beads were separated from the solution by filtration, thoroughly washed with deionized water and dried at room temperature. Finally, the HA-alginate-SWCNT products contained 0.05% and 0.5% (w/w) of SWCNTs in relation to the HA powder. Subsequently, samples were denoted as HA–alginate–0.05SWCNT and HA–alginate–0.5SWCNT, respectively. SWCNT-free sample was synthesized by the above technology and used as a control. It was denoted as HA–alginate.

Analytical methods and computer calculation

TEM analysis

The structure of the fabricated SWCNTs was examined using a transmission electron microscope (TEM, FEI Titan) operating at 80–300 kV.

SEM analysis

Experiments were carried out using a scanning electron microscope (SEM, REMMA-102), produced by SELMI (Ukraine). Microphotographs of the surface of the samples were made in the secondary electron mode with an accelerating voltage $U_{ac} = 20$ kV and a beam current of 1–10 A. The preparation consisted in spraying the conducting layer of silver onto the surface of the sample with a vacuum post VUP-5M (SELMI).

XRD analysis

The X-ray diffraction (XRD) studies of the prepared samples were performed using the automatized diffractometer Shimadzu XRD-6000 with Cu-Kα radiation. The scanning data were collected in the continuous registration mode into 2θ range (5.0–60.0°) with step of 0.02° and counting time of 2 s. Identification of the crystal phases was performed using the JCPDS (Joint Committee on Powder Diffraction Standards) card catalog. The average crystallite sizes (L, in nm) along (002) directions were estimated by the Scherrer equation. Calculation of the hexagonal lattice parameters, a and c, was held by the corresponding formulas, using the Miller indexes. Microstrain level ε was measured as the change in interplane distances of the crystals. Physical extension of diffraction lines occurs only through the crystal lattice microstrain, hence, ε level is determined as

$$\varepsilon = \frac{\beta_n}{4\mathrm{tg}\theta}, \tag{1}$$

where β_n is the integral width of the diffraction profile, in which physical extension occurs only through the crystal lattice microstrain (Klug and Alexander 1974; Kuznetsov et al. 2014).

FTIR analysis

Fourier-transform infrared spectra (FTIR) were obtained with a Perkin&Elmer Spectrum BX spectrometer. Samples were prepared in the form of KBr discs. Spectra were recorded over the range 4000–400 cm^{-1} at 1 cm^{-1} resolution.

Structural modeling

The spatial structure of the elementary cell of HA was reported in (Wilson et al. 1999) from X-ray analysis of the synthetic H6L sample, and was taken by us from the American Mineralogist Crystal Structure Database in the form of AMC-file (code 0002297). This cell was further used to construct flat crystal structure comprising four 2×2 cells which well match the shape and dimensions of the corresponding rhomboid HA molecule, using the VESTA program (version 3.4.4) (Momma and Izumi 2011).

The structure of SWCNT with the length of 5 nm and diameter of ≈ 2 nm (1222 carbon atoms) was built using Nanotube Modeler 1.8.

The structure of alginate was built using HyperChem 8.0 software (the Sugar Builder module) by alternating hyaluronic (HYL) and mannuronic (MAN) units, linked by α-1,4 glycosidic bonds. The length of the oligosugar was set in a way to cover the perimeter of the interface between HA

and SWCNT and comprised 17 units: $(HYL\text{-}MAN)_8\text{-}HYL$. The hydrogen atoms of sugar carboxyls were substituted by sodium atoms.

The structure of the HA–alginate–SWCNT system was built using HyperChem 8.0 software and energy minimized using the molecular mechanics method MM+.

Ca/P molar ratio

The Ca/P ratio was determined using the energy-dispersive X-ray fluorescence spectrometer ElvaX Light SDD. The voltage of the Rh anode X-ray tube was 12 kV. Samples were placed in a powder form inside small hollow cylindrical containers covered from one side with a special X-ray transparent film. The container was placed with its covered side on the top of the tube-detector window, and was blown by helium gas for more accurate measurements of the concentrations of light elements. Calcium and phosphorous concentrations were estimated only for HA samples by the regression analysis method.

Swelling (water uptake) and retention ability

The swelling was quantified by measuring the sample weight changes as a function of immersion time in the phosphate buffered saline (PBS). This was a water-based salt solution containing disodium hydrogen phosphate (10 mmol/L), sodium chloride (137 mmol/L), potassium chloride (2.7 mmol/L) and potassium dihydrogen phosphate (1.8 mmol/L) (Sukhodub et al. 2018; Palasz et al. 2008). The appropriate quantity of each component was dissolved in 1 L of distilled water to obtain the needed concentration. The osmolarity and ion concentrations of these solutions match those of the human saline.

Dried beads with a mass of 0.1 g (W_o) were immersed in PBS for 48 h. Samples were then carefully removed from the solution and placed on a filter paper for 5 min, followed by weighing (W_t) to determine the absorption of liquid (swelling; S_w) (Han et al. 2013) as

$$S_w = \frac{(W_t - W_0)}{W_0} \times 100\%, \tag{2}$$

where W_0 is the initial sample weight, and W_t is the final weight of the swollen sample.

To measure the water retention ability, the wet beads were transferred to centrifuge tubes with filter paper at the bottom, centrifuged at 600 rpm for 5 m and weighed immediately (W_t'). Percentages of water retention (E_r) of beads at equilibrium were calculated using the following equation (Venkatesan et al. 2011):

$$E_r = \frac{(W_t' - W_0)}{W_0} \times 100\%. \tag{3}$$

Compressive strength

HA-based composites were prepared in the form of tablets with diameter 5 mm and a thickness 2.25–2.35 mm by cold pressing method using the hydraulic press (at ~ 100 MPa). Measurement of the strength under a uniaxial compression was done in dry condition using the original automated equipment (Vovchenko et al. 2014).

Drug release kinetics

The material composition influence on the drug release was investigated in this experiment. The pharmaceutical AnS solution with concentration 11.00 mg/mL was used as a model drug. The experimental beads were saturated with AnS solution for 2 days followed by drying at 37 °C. For the drug release test, the 0.15 g of each sample, namely HA-alginate, HA–alginate–0.05SWCNT and HA–alginate–0.5SWCNT, saturated with AnS, was placed into 6.0 mL of PBS (pH 7.4) and incubated at 37 °C with continuing shaking at 80 rpm. The rate of drug release from composites was determined by taking 600 μL aliquots of PBS from each experimental tube daily for 20 days. An equal volume of the fresh medium was added back to maintain a constant initial volume in tubes. To determine the maximum amount of drug released, 0.15 g of each AnS-saturated sample was placed in separate PBS control tubes. Throughout the study period, the tubes were under the same conditions as the experimental tubes, but without the addition of fresh PBS. After 480 h, PBS was separated by centrifugation and the released AnS was determined by the high-performance liquid chromatography (HPLC; Agilent Technologies 1200, detector with UV–Vis Abs, detection at $\lambda = 280$ nm, column C18 (Zorbax SB-C18 4.6×150 mm, 5 μm)). The data acquisition and processing was done with Empower 2 software. The following mobile phase was used: methanol and 10% v/v glacial acetic acid (10:90). Isocratic treatment was applied at a rate of elution 2 mL/min with the temperature of analytical column 40 °C. The method of eluent components pre-mixing followed by 30 min sonication was applied to reduce errors in measuring of the substance with small component concentrations.

Cell viability assay

Primary human osteoblast cell culture was cultured in Dulbecco's Modified Eagle Medium/Nutrient Mixture F-12 (DMEM/F-12) with L-glutamine used, containing 100 units/

mL penicillin, 100 μg/mL streptomycin, 2.5 μg/mL amphotericin B, 10% Fetal Bovine Serum (FBS) and 1.0 ng/mL bFGF. Cells were maintained at 37 °C in a humidified incubator with 5% CO_2 for 24 h, until a monolayer, with greater than 80% confluence, was obtained. Osteoblasts were seeded in each well at a cell density of (4×10^4 cells per well). After 24 h cell cultivation, cdHA–alginate–SWCNT and cdHA–alginate were added into wells weighing 0.026–0.028 g.

Cell viability was analyzed by the colorimetric Alamar blue assay in which resazurin is a blue dye reduced to the pink-colored resorufin only by viable mitochondria. Alamar blue (Invitrogen) was added in an amount equal to 10% of the volume to each well. As negative control, Alamar Blue solution was added to the medium without cells. As a positive control, Alamar blue solution was added to the medium for which wells contained only cells without samples (tissue culture plastic control). Plates were incubated for 4 h at 37 °C in the dark. The medium was transferred to another 96-well plate and absorbance was measured using a Multiscan FC (Thermo Fisher Scientific) plate reader at wavelengths of 570 and 600 nm. The cell viability was measured on the 1st and 3rd days of cells cultivation. All experiments were repeated three times. The calculation of the percentage of Alamar blue reduction was performed according to the manufacturer's protocol (Mansour and Bickle 2010). Cell growth and proliferation controlled using EVOS XL Core cell imaging system (ThermoFisher Scientific, USA) on day 3 after co-cultivation.

Statistical analysis

Swelling degree, water retention, drug release, mechanical characteristics of the samples, and the cell viability test were performed in triplicate. Error bars for experimental values represent the range of obtained values. Student t test was used to analyze whether there were any statistical differences in the ranges of the data at a 95% confidence level.

Results and discussion

Few goals were followed when preparing composite by combining HA, alginate and SWCNTs: (a) to create a homogeneous dispersion of SWCNTs in natural alginate polymer under ultrasonic treatment, ensuring uniform dispersion of SWCNTs throughout the composite and decreasing cytotoxicity of SWCNT, associated with their low homogeneity in the solution; (b) to induce interaction between HA and SWCNTs and enhance mechanical properties of the composite material; (c) to evaluate the composites as a drug carrier system with prolonged drug release ability.
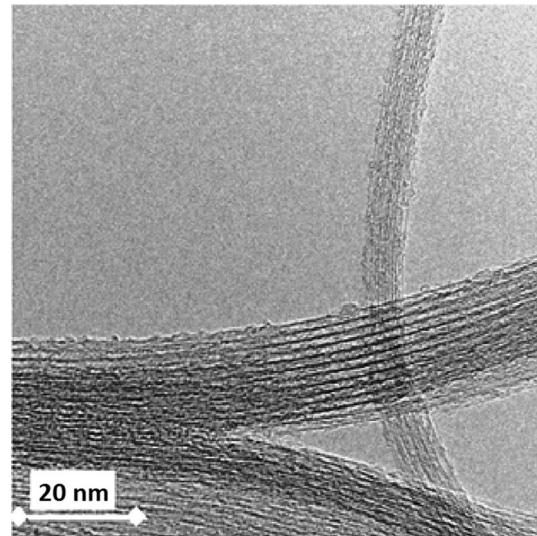

Fig. 1 TEM image of fabricated SWCNTs

According to the obtained electron microscopic micrographs (TEM; Fig. 1), the diameter and the length of fabricated SWCNTs appear to be 1–2 nm and 1–5 μm, respectively.

The microstructure of the composite beads was observed by SEM (Fig. 2). These images demonstrate a variety of bead surfaces. HA–alginate–0.05SWCNT and HA–alginate–0.5SWCNT beads are a 3D matrix consisting of alginate macromolecules cross-linked by calcium chloride, with HA immobilized in its structure, as well as 0.05% and 0.5% SWCNT particles. Figures show that increase of SWCNTs content leads to a denser structure. SEM images also represent a rusty surface with macro- (few μm) and micropores (< 1 μm), which is one of requirements for bioactive materials.

XRD investigations were carried out for the HA–alginate, HA–alginate–0.05SWCNT and HA–alginate–0.5SWCNT samples. As was mentioned above, the basis of the composite materials is the pre-synthesized HA hydrogel. The addition of carbon nanotubes did not affect the formation of HA crystallites. According to XRD patterns (not shown), HA contains nanoscale particles, as evidenced by the extension of reflexes from this sample. After its sintering at 900 °C, only single phase of HA with increasing crystallinity presents.

The average crystal size ($L_{Sherrer}$), calculated according to the Scherer's formula for diffraction peaks (002), as well as the lattice parameters, a and c, calculated in planes (002) and (211), are collected in Table 1. The calculation of crystal cell structure parameters showed slight deviation of the parameter a compared with the corresponding one for the stoichiometric HA ($a = 0.9421$ nm; $c = 0.6881$ nm). X-Ray fluorescence measurements have shown, that the Ca/P
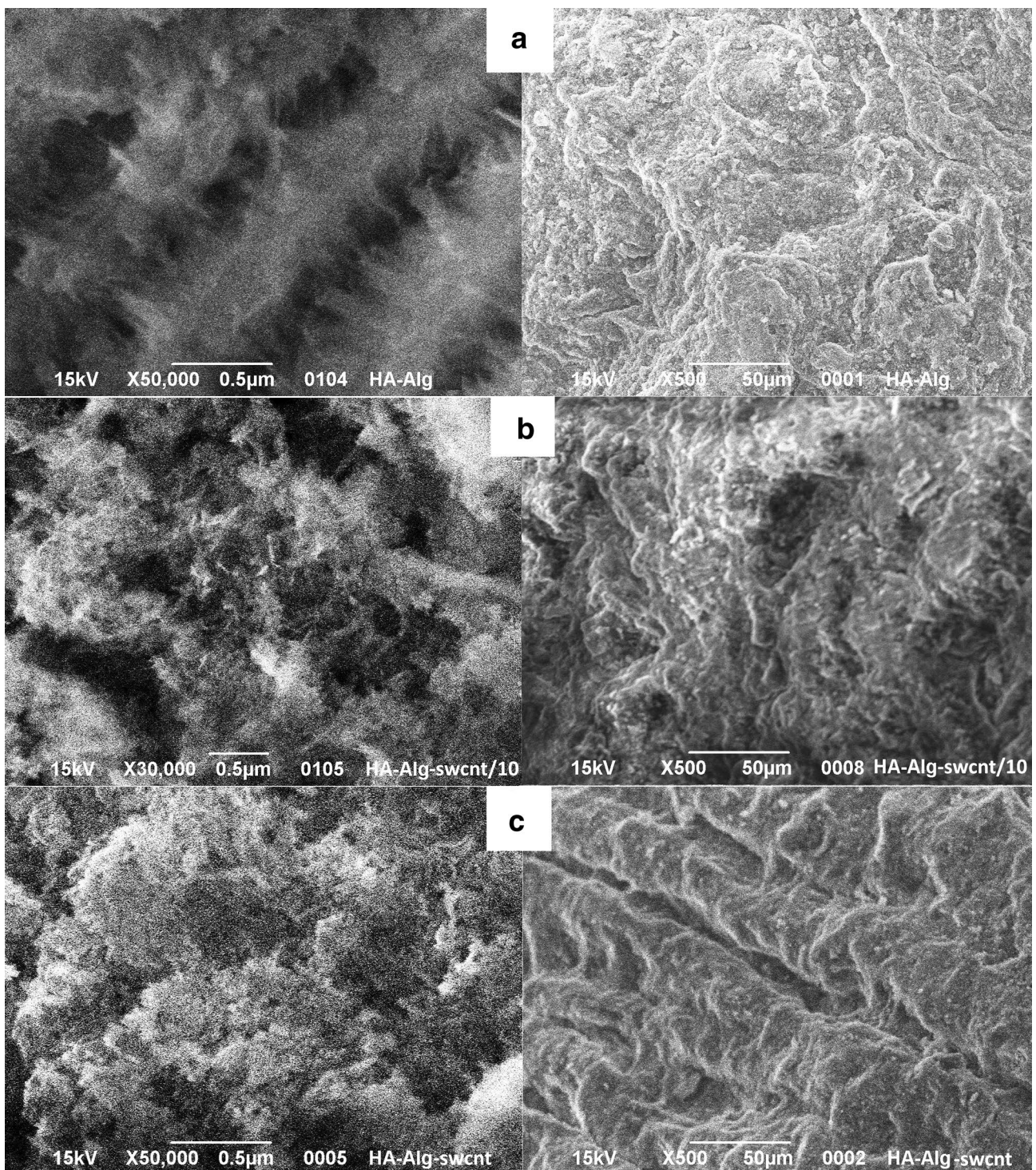
Fig. 2 SEM images of the samples surface: HA-alginate (**a**), HA-alginate-0.05SWCNT (**b**) and HA-alginate-0.5SWCNT (**c**) at different magnifications

atomic ratio in the obtained product is 1.65 ± 0.01, while for the stoichiometric HA, this ratio is 1.67. The obtained data indicate the formation of calcium deficient HA with small carbonate content. This fact is confirmed by further

FTIR studies that demonstrate the presence of the carbonate absorption bands at 870, 1420, and 1490 cm^{-1}. It could be assumed that carbonate ions from reactive solution were adsorbed by HA during the synthesis process. It is known

Table 1 Crystal structure parameters of HA-alginate-0.5SWCNT composite

Sample	$L_{Sherrer}$ (nm)							L_{CSR}[a] (nm)	Microstrain ε, 10^3	a (nm)	c (nm)
	(002)	(211)	(112)	(300)	(202)	(401)	(213)				
37 °C	25.5	–	–	–	–	–	–	23.0	1.839	0.938	0.6881
900 °C	37.4	28.7	25.9	26.3	37.4	29.7	35.2	33.8	0.497	0.940	0.6865

[a]L_{CSR} is the average mean of crystallite size for different planes

(Elliot 1994) that B-type carbonate apatite is characterized by the decrease of the lattice parameter *a*. The previous fact of the B-type carbonate apatite formation is confirmed by the FTIR spectra of the samples, where the vibrational mode of OH^- groups in HA at 630 cm^{-1} is not intensive and is overlapped by other vibrations. The value of microstrain (ε) is higher in the dried sample at 37 °C probably due to the presence of an organic component.

The characteristic IR bands of test samples are shown in Fig. 3. As it is evident, FTIR spectrum of the obtained HA-alginate composite shows characteristic vibration bands of the phosphate group PO_4 in HA in ranges of 1170–960 cm^{-1} (ν_3) and 610–550 cm^{-1} (ν_4). Bands at 3570 cm^{-1} and 630 cm^{-1} are assigned to stretching and vibrational modes of the hydroxyl group in apatite-type structure, respectively. A broad band in the range 3100–3500 cm^{-1} that covered the mode at 3570 cm^{-1} is associated with the absorbed water molecules. The presence of band at 1490, 1420 and 870 cm^{-1} of CO_3^{2-} modes indicates the partial substitution of phosphate by carbonate group and formation of B-type carbonated apatite. It should be noted that the band at 1420 cm^{-1} is due to overlapping of CO_3^{2-} modes with the symmetric stretching vibration of the COO^- groups of the alginate. The characteristic peak of alginate is also located at 1629 cm^{-1} and corresponding to asymmetric stretching vibration of carbonyl (C=O). Finally, it was found that an addition of SWCNT to HA–alginate composite does not affect the general pattern of FTIR spectrum. This result confirms the absence of chemical interaction between the SWCNT and HA–alginate molecular structure. Hence, one can assume the effect of physical adsorption between them in the form of binding the HA–alginate structure onto the SWCNT surface due to weak non-covalent stacking and van der Waals interactions.

The possibility of complexation between the studied compounds, SWCNT, HA and alginate, in aqueous mixture was testified by means of molecular mechanic calculations. The nearly flat shape of SWCNT and HA molecules suggests that in a mixture they likely form stacking-like complexes, whereas the triple HA–alginate–SWCNT complex features compact and stable structure if the alginate molecule encases the periphery of HA–SWCNT stack (Fig. 4). Modeling of such structure is an evidence of its stability in solution favored by solvophobic/van der Waals interactions between
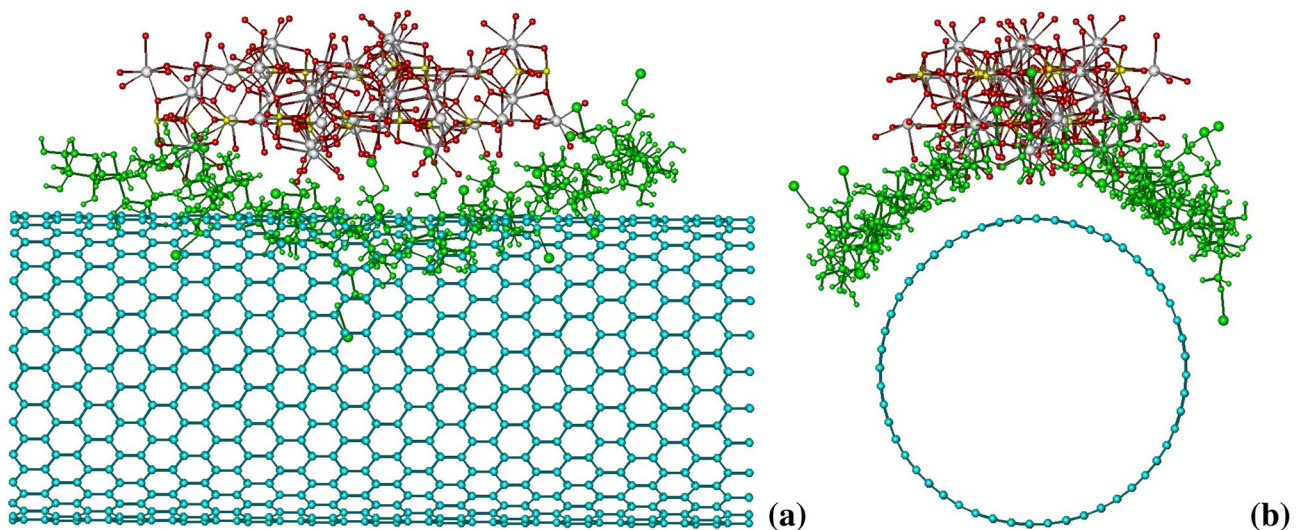
Fig. 3 FTIR spectra of the prepared samples
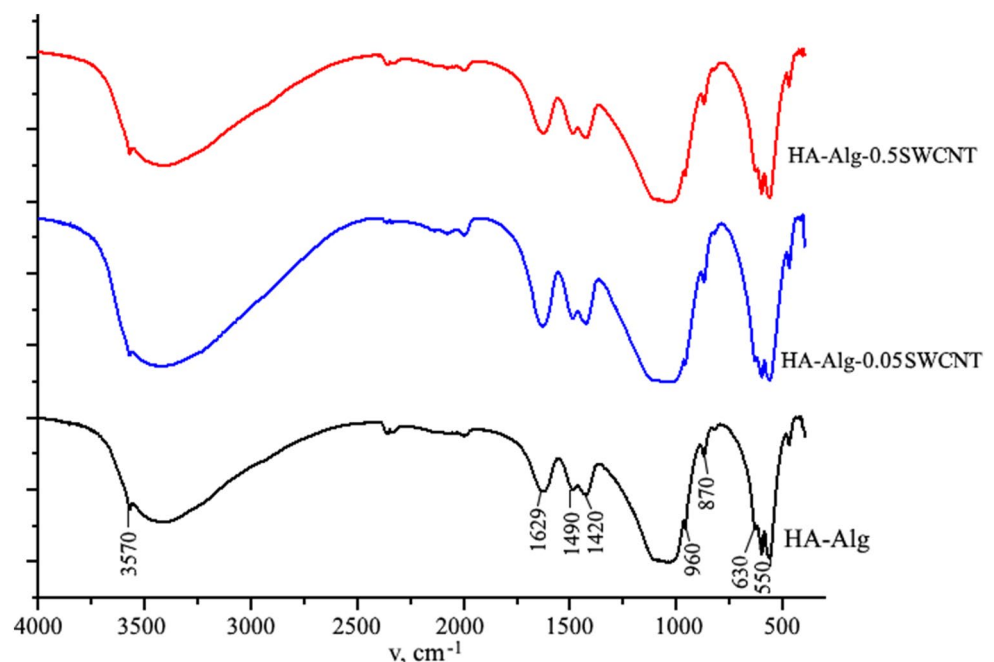
Fig. 4 Calculated spatial structures of HA-alginate-SWCNT triple complex (**a**, **b**—different views)
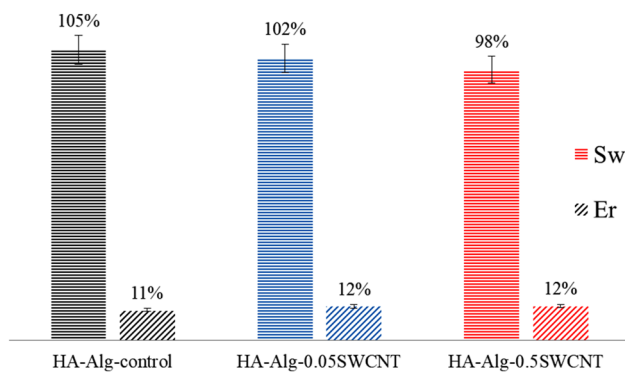

Fig. 5 Water uptake (swelling; S_w) and water retention (E_r) ability of HA-alginate, HA-alginate-0.05SWCNT and HA-alginate-0.5SWCNT composites after 24 h ($p \leq 0.05$)

the SWCNT and HA surfaces, and additionally stabilized by the hydrogen bonds between the OH-groups of alginate and oxygen atoms of HA (≈ 3 bonds). It thus may be concluded that the physical adsorption of SWCNT into HA–alginate system is possible by means of forming triple complexes stabilized by stacking interactions, H-bonds and solvophobic interactions.

Since the prepared nanocomposites are aimed for bone tissue engineering, the water uptake (swelling; S_w) and water retention (E_r) ability of the experimental beads are important factors. As it is evident from the obtained results (Fig. 5), the addition of SWCNTs to samples leads to lower degree of water absorption in proportion to the increase in the SWC-NTs content. Furthermore, the SWCNT-containing composites have significantly higher shape stability after agitation in the shaker (rpm 80) at 37 °C for 15 days. Herewith, water retention ability of all samples is comparable. This might be partially due to the hydrophobic character of SWCNTs. The shape stability and low value of swelling degree of SWCNT-containing samples suggest the potential use of this material for bone tissue engineering.

Results of the study of compressive strength for different types of HA-based composites are presented in Table 2, Fig. 6.

As it is observed in Fig. 6a, the addition of small content of SWCNT (0.05%) into HA–alginate composite slightly increases the compressive strength of the HA–alginate–0.05SWCNT sample compared to the HA–alginate control. The increase of SWCNT content by ten times (0.5%) in HA–alginate–0.5SWCNT sample leads to sufficient

Table 2 Strength properties of experimental composites

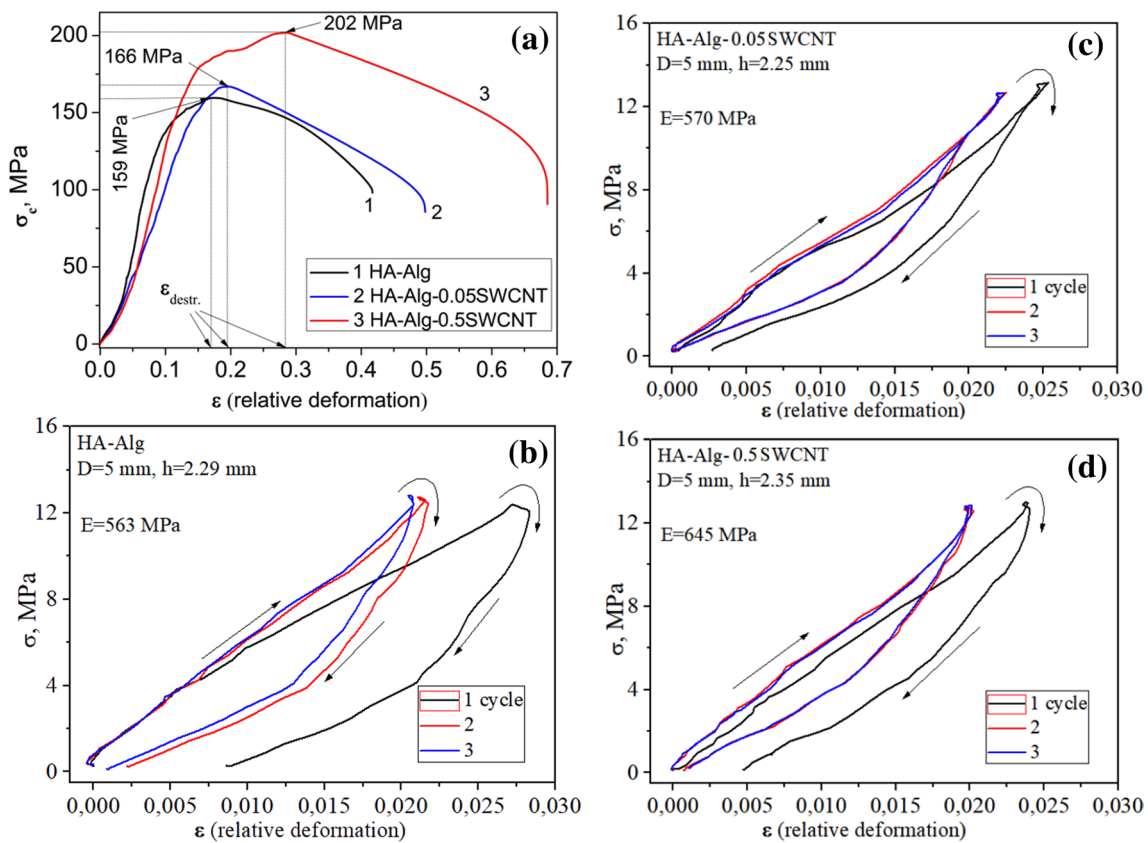| Sample	Density (g/cm³)	Maximal relative deformation, $\varepsilon_{\text{destr}}$	Strength σ_c (Mpa)	Young's modulus E (GPa)
HA-alginate	2.03 ± 0.03	0.17 ± 0.01	159 ± 7	0.563 ± 0.020
HA-alginate-0.05SWCNT	2.02 ± 0.03	0.19 ± 0.01	166 ± 7	0.570 ± 0.020
HA-alginate-0.5SWCNT	2.04 ± 0.04	0.28 ± 0.01	202 ± 9	0.645 ± 0.028

*$p \leq 0.05$

Fig. 6 Strength (σ_c) of the experimental composites (**a**); 'loading–unloading' diagrams during three loading cycles (**b**, **c**, **d**), measured at uniaxial compression

enhancement of its mechanical strength under compression up to 202 MPa. The maximal relative deformation, ε_{destr}, before destruction lies within the range of 0.17–0.19 for the HA–alginate and HA–alginate–0.05SWCNT samples. For the HA–alginate–0.5 SWCNT composite with highest SWCNT content the maximal relative deformations ε_{destr} increased up to 0.28.

Figure 6b, d represents the 'loading–unloading' diagrams of the investigated samples: HA-based composites were measured at uniaxial compression during the three loading cycles. Young's modulus is a measure of the stiffness of an elastic material and is a quantity used to characterize materials (Siddique and Mehta 2014). The Young's

modulus (E) estimation has shown that experimental composites have a comparatively high Young's modulus, namely $E \sim 0.563$–0.645 GPa (Table 2). For comparison, Table 3 shows the mechanical properties of cortical bone, synthetic HA and CNTs-containing composites.

In general, the increase of strength for HA–alginate samples with different contents of SWCNT is related to high aspect ratio (ranging from 1000 to 10 000) and excellent mechanical properties of SWCNT (a modulus of elasticity of 1 TPa or greater and a high tensile strength of up to 30 GPa) (Salvetat et al. 1999). A small change in compressive strength for the HA–alginate–0.05 SWCNT sample is explained by the small volume of interfacial areas of the

Table 3 Mechanical properties of cortical bone, synthetic HA and CNTs-containing composites

Mechanical characteristic	Cortical bone (Beladi and Saber-Samandari 2017; White et al. 2007)	Dense HA (Costa et al. 2012; Dorozhkin 2017; Ghomi et al. 2012; Roest et al. 2011)	Our data		
			HA-alginate	HA-alginate-MWCNT + Fe (Sukhodub et al. 2018)	HA-alginate-SWCNTs
Compressive strength (MPa)	100–230	100–215	159	168	202
Young's modulus (GPa)	10–25	0.25–10	0.563	0.74	0.645

HA–alginate–0.05SWCNT and ineffective process of loading transfer between HA–alginate and SWCNT. At the same time, the increase of SWCNT content (0.5%) provides a large volume of interfacial areas in HA–alginate–0.5SWCNT and increases compressive strength as a result of good interfacial adhesion between the composite components and efficient transferring the load from the HA–alginate matrix to the SWCNT, leading to the improvement of the mechanical properties (Gholami et al. 2014; Skwarek et al. 2017). On the other hand, it is known that the further increase of SWCNT content above certain concentration (> 1 wt%) (Khanal et al. 2016) may lead to SWCNT agglomeration that weakens the bonding between SWCNT and HA–alginate matrix and deteriorates the mechanical properties of HA–alginate–SWCNT composites.

The pharmaceutical Anaesthesinum (AnS) was introduced into composites by the method of saturation. AnS has an anesthetic effect, low toxicity, no side effects. It is easily soluble in alcohol, ether, chloroform, fats and fatty oils, very slightly soluble in water (1:2500). To evaluate the AnS release kinetics, 0.155 g of each drug containing experimental sample namely, HA–alginate, HA–alginate–0.05SWCNT and HA–alginate–0.5SWCNT, was placed into 6.0 mL of PBS (pH 7.4) and incubated at 37 °C with continuous agitation at 80 rpm for 480 h.

Figure 7a shows the chromatogram for the HA–alginate–0.5SWCNT sample with AnS peak, which reflects the retention time for AnS (8.9 min) and its concentration in PBS after 48 h exposure of test sample. This spectrum is typical, so the spectra of other samples are not shown. Another peak (1.6 min) on the chromatogram reflects the output of the partial degradation products that occurred over

48 h. The degree of sample degradation can be estimated by the area under the peak. Figure 7b shows the degradation ratio of all three samples under 408 h of exposure. It is seen that the greatest degradation is observed in the case of the HA–alginate control sample (15 mAU), and the smallest for HA–alginate–0.5SWCNT (2.38 mAU), which has the highest content of SWCNTs. It is noteworthy that after 48 h of exposure, the degradation ratio of all SWCNT-containing samples was unchanged—2.2 mAU.

The quantity of released AnS was plotted against the incubation time (Fig. 8). As noted above, the maximum possible AnS release is about 1.0 mg/mL. Therefore, the obtained concentration value in mg/mL can be easily converted into percentage, while the course of the curve will not change. The exception is the last period (408–480 h), where the percentage release of the drug is represented by a horizontal line.

Results showed that the AnS release from all experimental samples occurs almost uniformly throughout the study period and lasts for 408 h. After 408 h, the concentration of AnS in the PBS, released from HA–alginate and HA–alginate–0.05SWCNT, starts to decrease due to dilution, which occurs by adding the aliquots of fresh PBS solution after each sampling, while AnS is no longer released. At the same time, the AnS concentration in the tube with HA–alginate–0.5SWCNT remains constant for further 48 h, and only after this time starts to decrease. The AnS release from the samples took place evenly throughout the study period. The graphic diagram (Fig. 8) shows that the drug release occurred at a lower average rate from the SWCNT-containing samples (1.28 µg/h) compared to the HA–alginate control (1.33 µg/h). This can be explained by the additional
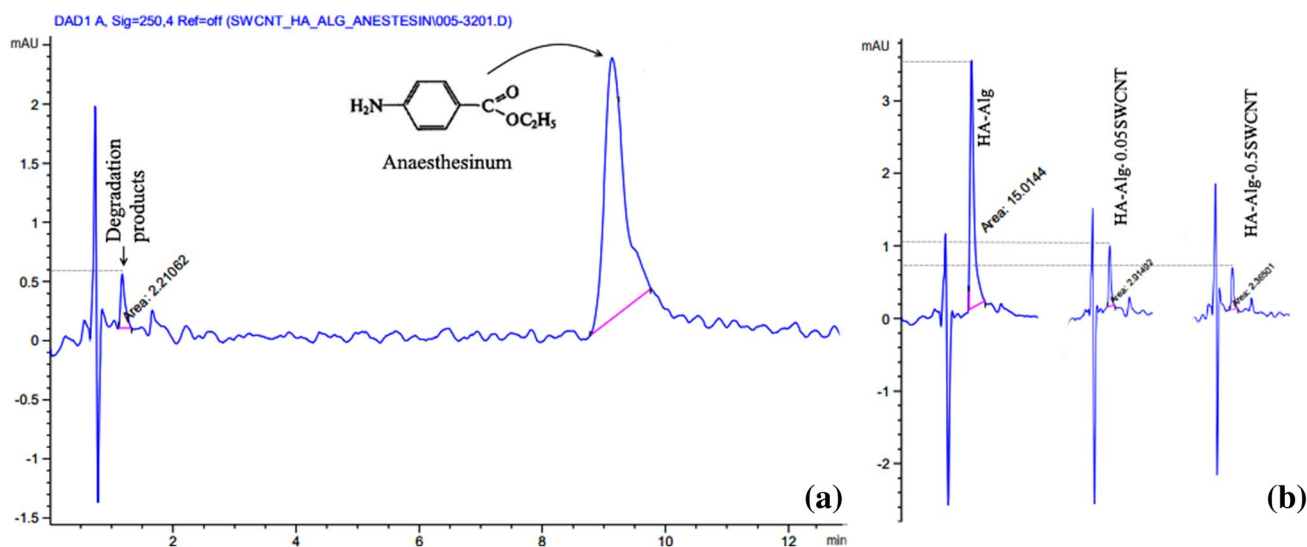

Fig. 7 HPLC pattern from test samples: release of AnS from HA-alginate-0.5SWCNT (**a**); release of the degradation products in 408 h of sample exposure (**b**)
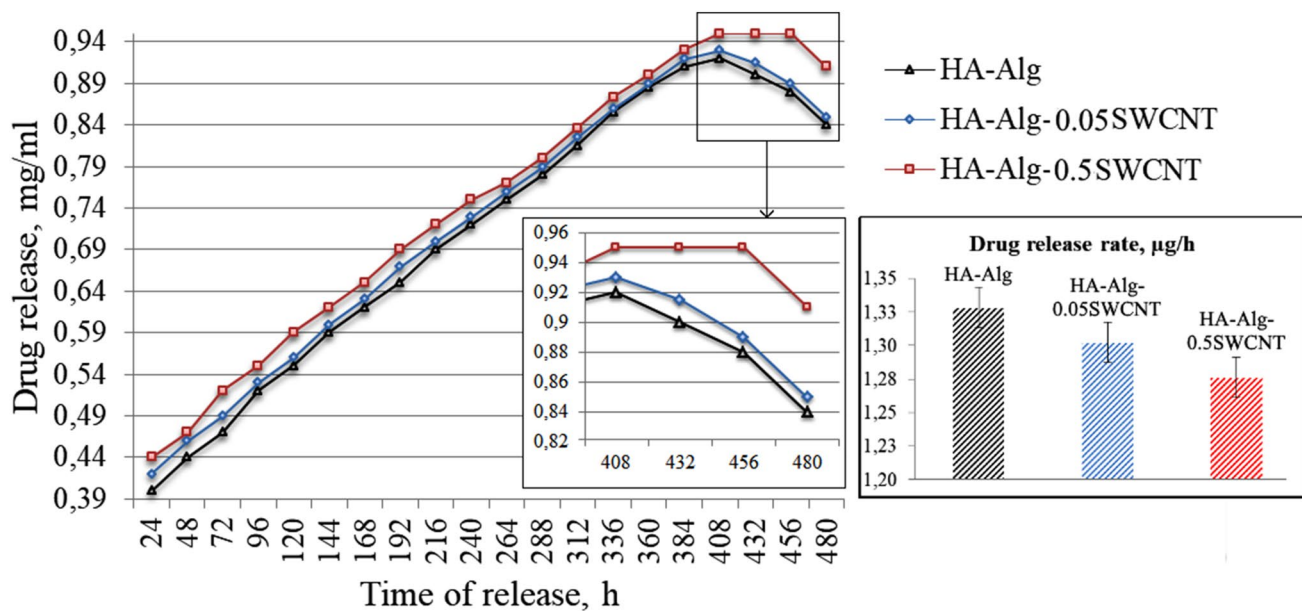
Fig. 8 Concentration of AnS in PBS (μg/mL), released from the experimental samples for 480 h ($p \leq 0.05$)

binding of AnS to the surface of SWCNTs. The partial biodegradation of the polymer matrix leads to the instability of the scaffold shape that influences the release of the drug. The drug release rate in general depends on the solubility of the drug and degradation of the matrix, the possibility of a diffusion process, the rate of the drug diffusion through the matrix and the desorption of the surface-linked or adsorbed drug. Thus, the solubility, diffusion and biodegradation of the matrix particles regulate the drug release process. In the experimental samples, where the drug is distributed in whole scaffold bulk, the drug release may occur by both the diffusion process and erosion of the matrix. From the shape stability test, we can see, that the drug release is faster than the erosion of the matrix, so the mechanism of AnS release is mainly controlled by a diffusion process. In addition, the drug molecules are bound with SWCNTs by the van der Waals couplings or adsorbed on their surface. Therefore, SWCNTs can act as a certain barrier that regulates prolonged drug release.

Osteoblast cell culture assay showed no cell toxicity for both HA–alginate and HA–alginate–0.5SWCNT samples (Fig. 9). A 24-h cultivation showed satisfactory cell adhesion between $85.4 \pm 3.7\%$ and $92.5 \pm 7.3\%$ with no significant difference with tissue culture plastic control group ($89.6 \pm 6.8\%$). A 3-day cultivation indicates better osteoblast proliferation with the experimental composites compared to the tissue culture plastic, that is, probably, due to specific stimuli from the HA and alginate present in composites. On the 3rd day, one can see complete cell confluence both on HA–alginate and HA–alginate–0.5SWCNT samples. Remnants of the degradation products are visualized between osteoblasts and no penetrated cell membrane. Osteoblasts have typical morphology with intercellular communication that additionally suggests biocompatibility of both HA–alginate and HA–alginate–0.5SWCNT composites.

Conclusion

SWCNTs containing biomaterial with enhanced mechanical properties for the potential orthopedic application was synthesized and investigated. Composites were synthesized in form of beads and present as 3D matrix consisting of alginate macromolecules cross-linked by calcium ions, with HA immobilized in its structure as well as 0.05% and 0.5% SWCNTs particles. XRD and X-ray fluorescence analysis indicate the formation of calcium-deficient ($Ca/P = 1.65 \pm 0.01$) HA with a small carbonate content under influence of MW irradiation. The investigated mechanical properties (maximal relative deformation, compressive strength and Young's modulus) of SWCNT loaded HA–alginate composites confirm their dependence on the SWCNTs content. The compressive strength of HA–alginate–SWCNT and HA–alginate control (202 and 159 MPa, respectively) lies within the values typical for the cortical bone. The addition of 0.5% of SWCNT in relation to the content of HA increases the Young's modulus of the HA–alginate–SWCNT (645 MPa) compared to the SWCNT-free HA–alginate sample (563 MPa) and enhances the material shape stability in simulated physiologic conditions. Structural modeling
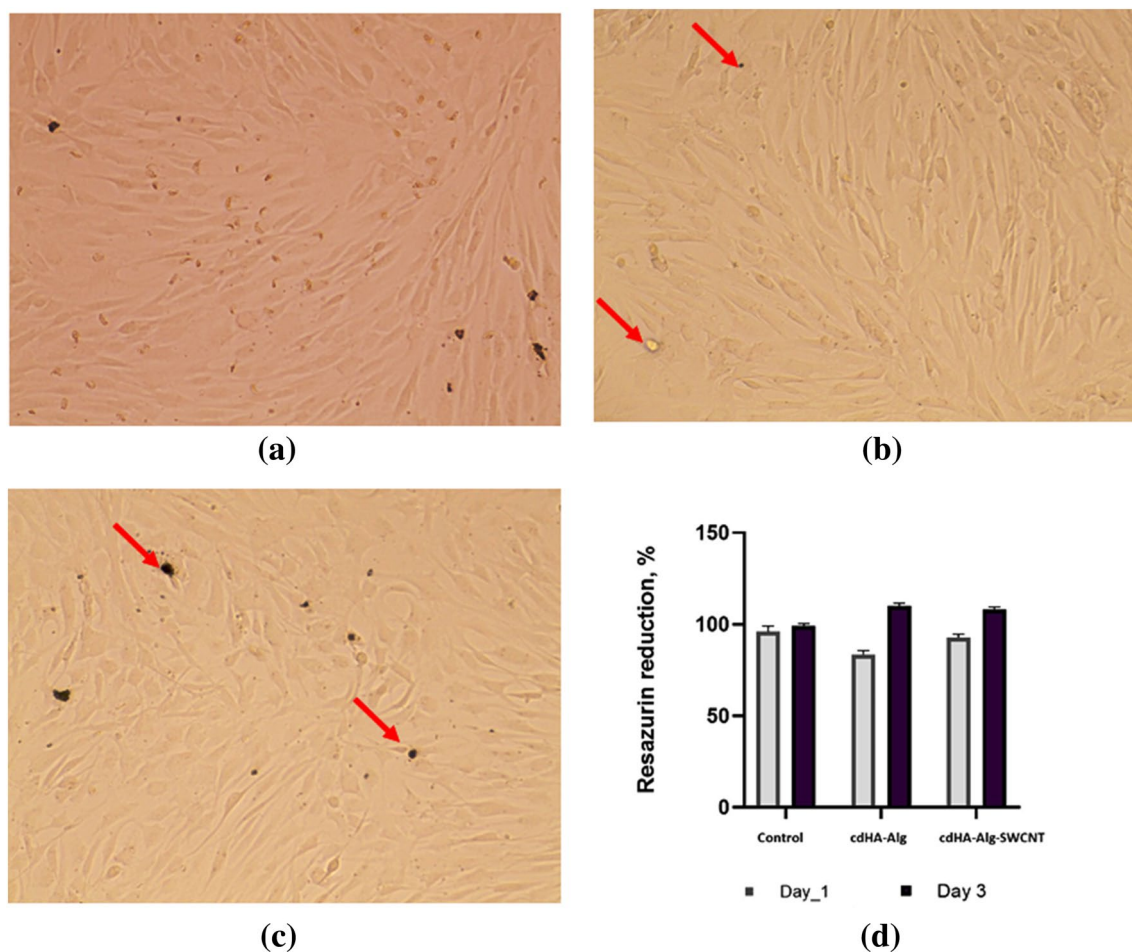
Fig. 9 Optical images of cell human primary osteoblasts on day 3 after cultivation on tissue culture plastic (**a**), HA-alginate (**b**) and HA-alginate-0.5SWCNT (**c**) and *Resazurin* reduction data on day 1 and day 3 (**d**) ($p \leq 0.05$). Red arrows show the degradation products

of HA–alginate–SWCNT system showed that physical adsorption of SWCNT into HA–alginate occurs by forming triple complexes stabilized by solvophobic/van der Waals interactions and H-bonds. The HPLC study demonstrates the influence of SWCNTs on the prolonged AnS release (456 h against 408 h for SWCNT-free sample). Cell culture assay confirms biocompatibility and stimulation of osteoblast proliferation of 0.05% and 0.5% SWCNTs-containing composites during the 3 day cultivation. These facts suggest the potential possibility of usage of SWCNT-containing materials, based on HA and alginate, for bone tissue engineering.

Author contributions LFS and YIP: managing the experiment, drafting the manuscript; LBS, MOK and MVP: preparation, characterization and biotesting of composite materials; MPE and VVK: computer simulation; YIP, NYS and LLV: FTIR analysis and mechanical properties; UR and SVK: preparation and characterization of SWCNTs; LFS: design of the study, general supervision.

Compliance with ethical standards

Conflict of interest The authors declare that they have no conflict of interest.

Ethical approval This article does not contain any studies with human participants or animals performed by any of the authors.

References

Andón FT, Fadeel B (2013) Programmed cell death: molecular mechanisms and implications for safety assessment of nanomaterials. Acc Chem Res 46:733–742

Beladi F, Saber-Samandari S (2017) Cellular compatibility of nanocomposite scaffolds based on hydroxyapatite entrapped in cellulose network for bone repair. Mater Sci Eng C 75:385–392

Beyer M, Reichert J, Heurich E, Jandt KD, Sigusch BW (2010) Pectin, alginate and gum arabic polymers reduce citric acid erosion effects on human enamel. Dent Mater J 26:831–839

Boontheekul T, Kong HJ, Mooney DJ (2005) Controlling alginate gel degradation utilizing partial oxidation and bimodal molecular weight distribution. Biomaterials 26:2455–2465

Buchelnikov AS, Voronin DP, Kostjukov VV, Deryabina TA, Khrapatiy SV, Prylutskyy YuI, Ritter U, Evstigneev MP (2014) Complexation of aromatic drugs with single-walled carbon nanotubes. J Nanopart Res 16:2472

Cataldo F, Da Ros T (2008) Medicinal chemistry and pharmacological potential of fullerenes and carbon nanotubes. Springer Science & Business Media, Berlin

Constanda S, Stan MS, Ciobanu CS, Motelica-Heino M, Guégan R, Lafdi K, Dinischiotu A, Predoi D (2016) Carbon nanotubes-hydroxyapatite nanocomposites for an improved osteoblast cell response. J Nanomater 2016:Article ID 3941501

Costa DO, Allo BA, Klassen R, Hutter JL, Dixon SJ, Rizkalla AS (2012) Control of surface topography in biomimetic calcium phosphate coatings. Langmuir 28:3871–3880

Dorozhkin SV (2017) Calcium orthophosphates ($CaPO_4$): occurrence and properties. Morphologie 101:125–142

Elliot JC (1994) Structure and chemistry of the apatites and other calcium orthophosphates. Elsevier Science, Amsterdam-London-New York-Tokyo

Gholami F, Zein SHS, Ismail SB, Tan SH (2014) Cytocompatibility and mechanical properties of hydroxyapatite composite reinforced with multiwalled carbon nanotubes and bovine serum albumin. Chem Eng Sci 2:1–4

Ghomi H, Fathi MH, Edris H (2012) Effect of the composition of hydroxyapatite/bioactive glass nanocomposite foams on their bioactivity and mechanical properties. Mater Res Bull 47:3523–3532

Gopi D, Shinyjoy E, Sekar M, Surendiran M, Kavitha L, Kumar TS (2013) Development of carbon nanotubes reinforced hydroxyapatite composite coatings on titanium by electrodeposition method. Corrosion Sci 73:321–330

Han Y, Zeng Q, Li H, Chang J (2013) The calcium silicate/alginate composite: preparation and evaluation of its behavior as bioactive injectable hydrogels. Acta Biomater 9:9107–9117

Harik VM (2017) Geometry of carbon nanotubes and mechanisms of phagocytosis and toxic effects. Toxicol Lett 273:69–85

Iijima S (1991) Helical microtubules of graphitic carbon. Nature 354:56–58

Jorio A, Dresselhaus G, Dresselhaus MS (2007) Carbon nanotubes: advanced topics in the synthesis, structure, properties and applications. Springer Science & Business Media, Berlin

Kam NWS, O'Connell M, Wisdom JA, Dai H (2005) Carbon nanotubes as multifunctional biological transporters and near-infrared agents for selective cancer cell destruction. Proc Natl Acad Sci USA 102:11600–11605

Khalid P, Hussain MA, Rekha PD, Arun AB (2013) Synthesis and characterization of carbon nanotubes reinforced hydroxyapatite composite. Indian J Sci Technol 6:5546–5551

Khanal SP, Mahfuz H, Rondinone AJ, Leventouri Th (2016) Improvement of the fracture toughness of hydroxyapatite (HAp) by incorporation of carboxyl functionalized single walled carbon nanotubes (CfSWCNT) and nylon. Mater Sci Eng C 60:204–210

Klug HP, Alexander LE (1974) X-ray diffraction procedures: for polycrystalline and amorphous materials. Wiley, New York

Korolovych VF, Bulavin LA, Prylutskyy YuI, Khrapatiy SV, Tsierkezos N, Ritter U (2014) Influence of single-walled carbon nanotubes on the thermal expansion of water. Int J Thermophys 35:19–31

Kurantowicz N, Sawosz E, Halik G, Strojny B, Hotowy A, Grodzik M, Piast R, Pasanphan W, Chwalibog A (2017) Toxicity studies of six types of carbon nanoparticles in a chicken-embryo model. Int J Nanomed 12:2887–2898

Kuznetsov VM, Sukhodub LB, Sukhodub LF (2014) Structural and substructural features of apatite-biopolymer composites: the comparison of data obtained using X-ray diffraction and scanning electron microscopy with electron diffraction. J Nano-Electron Phys 6:04039

Lee KY, Mooney DJ (2012) Alginate: properties and biomedical applications. Prog Polym Sci 37:106–126

Li Z, Ramay HR, Hauch KD, Xiao D, Zhang M (2005) Chitosan-alginate hybrid scaffolds for bone tissue engineering. Biomaterials 26:3919–3928

Li A, Sun K, Dong W, Zhao D (2007) Mechanical properties, microstructure and histocompatibility of MWCNTs/HAp biocomposites. Mater Lett 61:1839–1844

Li Q, Liu J, Xu S (2015) Progress in research on carbon nanotubes reinforced cementitious composites. Adv Mater Sci Eng 2015:Article ID 307435

Li Z, Bi S, Thompson BC, Li R, Khor KA (2017) Multifunctional bioceramic-based composites reinforced with silica-coated carbon nanotube core-shell structures. Ceramics Int 43:16084–16093

Liu Z, Tabakman S, Welsher K, Dai H (2009) Carbon nanotubes in biology and medicine: *in vivo* and *in vitro* detection, imaging and drug delivery. Nano Res 2:85–120

Mansour NR, Bickle QD (2010) Comparison of microscopy and Alamar blue reduction in a larval based assay for schistosome drug screening. PLoS Negl Trop Dis 4:795

Matyshevska OP, Karlash AYu, YaV S, Benilov A, Kirgizov Yu, Gorchinskyy KO, Buzaneva EV, Prylutskyy YuI, Scharff P (2001) Self-organizing DNA/carbon nanotube molecular films. Mater Sci Eng C 15:249–252

Minchenko OH, Tsymbal DO, Minchenko DO, Prylutska SV, Hnatiuk OS, Prylutskyy YuI, Tsierkezos N, Ritter U (2018) Single-walled carbon nanotubes affect the expression of genes associated with immune response in normal human astrocytes. Toxicol In Vitro 52:122–130

Momma K, Izumi F (2011) VESTA 3 for three-dimensional visualization of crystal, volumetric and morphology data. J Appl Crystallogr 44:1272–1276

Palasz AT, Breña PB, De-la-Fuente J, Gutiérrez-Adán A (2008) The effect of different zwitterionic buffers and PBS used for out-of-incubator procedures during standard *in vitro* embryo production on development, morphology and gene expression of bovine embryos. Theriogenology 9:1461–1470

Prylutska SV, Grynyuk II, Matyshevska OP, Yashchuk VM, Prylutskyy YuI, Ritter U, Scharff P (2008) Estimation of multi-walled carbon nanotubes toxicity *in vitro*. Physica E 40:2565–2569

Prylutska S, Bilyy R, Schkandina T, Bychko A, Cherepanov V, Andreichenko K, Stoika R, Rybalchenko V, Prylutskyy Yu, Scharff P, Ritter U (2012) Effect of iron-doped multi-walled carbon nanotubes on lipid model and cellular plasma membranes. Mater Sci Eng C 32:1486–1489

Prylutska S, Bilyy R, Shkandina T, Rotko D, Bychko A, Cherepanov V, Stoika R, Rybalchenko V, Prylutskyy Yu, Tsierkezos N, Ritter U (2013) Comparative study of membranotropic action of single- and multi-walled carbon nanotubes. J Biosci Bioeng 115:674–679

Radchenko NV, Prylutskyy YI, Shapoval LM, Sagach VF, Davydovska TL, Dmitrenko OV, Stepanenko LG, Pobigailo LS, Schütze C, Ritter U (2013) Impact of single-walled carbon nanotubes on the medullary neurons in spontaneously hypertensive rats. Mat Wiss u Werkstofftech 44:171–175

Raphey VR, Henna TK, Nivitha KP, Mufeedha P, Sabu C, Pramod K (2019) Advanced biomedical applications of carbon nanotube. Mater Sci Eng C 100:616–630

Reich S, Thomsen C, Maultzsch J (2008) Carbon nanotubes: basic concepts and physical properties. Wiley, New York

Ritter U, Scharff P, Dmytrenko OP, Kulish NP, Prylutskyy YuI, Belyi NM, Gubanov VA, Komarova LA, Lizunova SV, Shlapatskaya

VV, Bernas H (2007) Radiation damage and Raman vibrational modes of single-walled carbon nanotubes. Chem Phys Lett 447:252–256

Ritter U, Tsierkezos NG, Prylutskyy YuI, Matzui LYu, Gubanov VO, Bilyi MM, Davydenko MO (2012) Structure-electrical resistivity relationship of N-doped multi-walled carbon nanotubes. J Mater Sci 47:2390–2395

Roest R, Latella BA, Heness G, Ben-Nissan B (2011) Adhesion of sol–gel derived hydroxyapatite nanocoatings on anodised pure titanium and titanium (Ti6Al4V) alloy substrates. Surf Coat Technol 205:3520–3529

Sakai S, Kawakami K (2007) Synthesis and characterization of both ionically and enzymatically cross-linkable alginate. Acta Biomater 3:495–501

Salvetat J-P, Bonard J-M, Thomson NH, Kulik AJ, Forró L, Benoit W, Zuppiroli L (1999) Mechanical properties of carbon nanotubes. Appl Phys A 69:255–260

Sharma S, Srivastava D, Grover S, Sharma V (2014) Biomaterials in tooth tissue engineering: a review. J Clin Diagnost Res 8:309–315

Siddique R, Mehta A (2014) Effect of carbon nanotubes on properties of cement mortars. Construct Build Mater 50:116–129

Singla R, Sharma C, Shukla AK, Acharya A (2019) Toxicity concerns of therapeutic nanomaterials. J Nanosci Nanotechnol 19:1889–1907

Skwarek E, Bolbukh Yu, Janusz W, Tertykh V (2017) Hydroxyapatite composites with multiwalled carbon nanotubes. Adsorpt Sci Technol 35:534–544

Stanislavov AS, Sukhodub LF, Sukhodub LB, Kuznetsov VN, Bychkov KL, Kravchenko MI (2018) Structural features of hydroxyapatite and carbonated apatite formed under the influence of ultrasound and microwave radiation and their effect on the bioactivity of the nanomaterials. Ultrason Sonochem 42:84–96

Sukhodub LF, Sukhodub LB, Litsis OO, Prylutskyy YuI (2018a) Synthesis and characterization of hydroxyapatite-alginate nanostructured composites for the controlled drug release. Mater Chem Phys 217:228–234

Sukhodub LB, Sukhodub LF, Prylutskyy YuI, Strutynska NYu, Vovchenko LL, Soroca VM, Slobodyanik NS, Tsierkezos NG, Ritter U (2018b) Composite material based on hydroxyapatite and multi-walled carbon nanotubes filled by iron: preparation, properties and drug release ability. Mater Sci Eng C 93:606–614

Tang Y, Zhao K, Hu L, Wu Z (2013) Two-step freeze casting fabrication of hydroxyapatite porous scaffolds with bionic bone graded structure. Ceram Int 39:9703–9707

Tran PA, Zhang L, Webster TJ (2009) Carbon nanofibers and carbon nanotubes in regenerative medicine. Adv Drug Deliv Rev 61:1097–1114

Van Dijk HJA, Hattu N, Prijs K (1981) Preparation, microstructure and mechanical properties of dense polycrystalline hydroxyapatite. J Mater Sci 16:1592–1598

Venkatesan J, Qian ZJ, Ryu BM, Ashok N, Kim SK (2011) Preparation and characterization of carbon nanotube-grafted-chitosan – natural hydroxyapatite composite for bone tissue engineering. Carbohyd Polym 83:569–577

Vovchenko L, Lazarenko O, Matzui L, Perets Yu, Zhuravkov A, Fedorets V, Le Normand F (2014) Mechanical and electrical properties of the epoxy composites with graphite nanoplatelets and carbon nanotubes. Phys St Sol A 211:336–341

White AA, Best SM, Kinloch IA (2007) Hydroxyapatite-carbon nanotube composites for biomedical applications: a review. Int J Appl Ceramic Technol 4:1–13

Wilczewska AZ, Niemirowicz K, Markiewicz KH, Car H (2012) Nanoparticles as drug delivery systems. Pharmacol Rep 64:1020–1037

Wilson RM, Elliot JC, Dowker SEP (1999) Rietveld refinement of the crystallographic structure of human dental enamel apatites. Am Mineralogist 84:1406–1414